university of groningen

University Medical Center Groningen

University of Groningen

Heterostructure from PbS Quantum Dot and Carbon Nanotube Inks for High-Efficiency Near-Infrared Light-Emitting Field-Effect Transistors

Bederak, Dmytro; Shulga, Artem; Kahmann, Simon; Talsma, Wytse; Pelanskis, Jokūbas; Dirin, Dmitry N.; Kovalenko, Maksym V.; Loi, Maria A.

Published in:
Advanced electronic materials

DOI:
10.1002/aelm.202101126

IMPORTANT NOTE: You are advised to consult the publisher's version (publisher's PDF) if you wish to cite from it. Please check the document version below.

Document Version
Publisher's PDF, also known as Version of record

Publication date:
2022

Link to publication in University of Groningen/UMCG research database

Citation for published version (APA):
Bederak, D., Shulga, A., Kahmann, S., Talsma, W., Pelanskis, J., Dirin, D. N., Kovalenko, M. V., & Loi, M. A. (2022). Heterostructure from PbS Quantum Dot and Carbon Nanotube Inks for High-Efficiency Near-Infrared Light-Emitting Field-Effect Transistors. *Advanced electronic materials*, *8*(7), [2101126]. https://doi.org/10.1002/aelm.202101126

Copyright
Other than for strictly personal use, it is not permitted to download or to forward/distribute the text or part of it without the consent of the author(s) and/or copyright holder(s), unless the work is under an open content license (like Creative Commons).

The publication may also be distributed here under the terms of Article 25fa of the Dutch Copyright Act, indicated by the “Taverne” license. More information can be found on the University of Groningen website: https://www.rug.nl/library/open-access/self-archiving-pure/taverne-amendment.

Take-down policy
If you believe that this document breaches copyright please contact us providing details, and we will remove access to the work immediately and investigate your claim.

Downloaded from the University of Groningen/UMCG research database (Pure): http://www.rug.nl/research/portal. For technical reasons the number of authors shown on this cover page is limited to 10 maximum.

Check for updates

ADVANCED ELECTRONIC MATERIALS
www.advelectronicmat.de

Heterostructure from PbS Quantum Dot and Carbon Nanotube Inks for High-Efficiency Near-Infrared Light-Emitting Field-Effect Transistors

*Dmytro Bederak, Artem Shulga, Simon Kahmann, Wytse Talsma, Jokūbas Pelanskis, Dmitry N. Dirin, Maksym V. Kovalenko, and Maria A. Loi**

Light-emitting field-effect transistors (LEFETs) are emerging optoelectronic devices able to display simultaneously electrical switching as transistors and electroluminescence emission as light emitting diodes. Lead chalcogenide colloidal quantum dots (CQDs) allow achieving light emission in a very broad spectral range, covering the near-infrared (NIR) and the short-wavelength infrared (SWIR) regions, which cannot be reached with other solution-processable materials. Therefore, the use of lead chalcogenide CQDs as active layer in LEFETs opens the possibility for very narrow and switchable light sources in the NIR and SWIR range. The recently reported, first fully solid-state lead chalcogenide (PbS) CQD based LEFET shows an electroluminescence (EL) quantum efficiency of 1.3×10^{-5} at room temperature and of about 1% below 100 K. To overcome the limits of a previous report, an active material comprising two sequentially deposited layers is designed, the first of PbS CQDs displaying n-type transport and the second of polymer-wrapped semiconducting carbon nanotubes displaying p-type dominated transport. With this double layer system, LEFETs displaying a well-balanced ambipolar transport, charge carrier mobility of about 0.2 $cm^2\ V^{-1}\ s^{-1}$ for both electrons and holes, and EL external quantum efficiency reaching 1.2×10^{-4} at room temperature are obtained.

1. Introduction

Colloidal quantum dots (CQDs) are solution-processable nanomaterials which have great potential for many applications in optoelectronics. Among the most desired properties are the large spectral tunability by size, the outstanding monodispersity and therefore color purity as well as the solution processability.[1–3] Due to the quantum confinement effect, the energetic position of the emission can be easily adjusted by tuning the size of the particles,[4] and their monodispersity give rise to a single narrow emission peak, which is at the base of their application in display technology (vide infra). Interestingly, the emission of CQDs can readily be extended to the near-infrared region (750–2500 nm) by using, for example, semiconductors display very narrow band gap in bulk, such as metal chalcogenides such as PbS and PbSe.[5] Near-infrared light has many important applications

D. Bederak,[+] A. Shulga,[+] S. Kahmann,[++] W. Talsma, J. Pelanskis, M. A. Loi
Zernike Institute for Advanced Materials
University of Groningen
Nijenborgh 4, Groningen 9747AG, The Netherlands
E-mail: m.a.loi@rug.nl

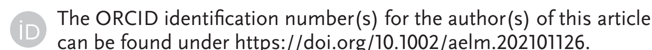
The ORCID identification number(s) for the author(s) of this article can be found under https://doi.org/10.1002/aelm.202101126.

© 2022 The Authors. Advanced Electronic Materials published by Wiley-VCH GmbH. This is an open access article under the terms of the Creative Commons Attribution License, which permits use, distribution and reproduction in any medium, provided the original work is properly cited.

[+]Present address: QDI Systems BV, L.J. Zielstraweg 1, Groningen 9713 GX, The Netherlands
[++]Present address: Cavendish Laboratory, University of Cambridge, Cambridge CB3 0HE, UK

DOI: 10.1002/aelm.202101126

D. N. Dirin, M. V. Kovalenko
Department of Chemistry and Applied Biosciences
ETH Zürich
Vladimir Prelog Weg 1, Zürich 8093, Switzerland
D. N. Dirin, M. V. Kovalenko
Empa-Swiss Federal Laboratories for Materials Science and Technology
Uberlandstrasse 129, Dübendorf 8600, Switzerland

 © 2022 The Authors. Advanced Electronic Materials published by Wiley-VCH GmbH

2199160x, 2022, 7, Downloaded from https://onlinelibrary.wiley.com/doi/10.1002/aelm.202101126 by Bibliotheek Rijksuniversiteit, Wiley Online Library on [18/01/2023]. See the Terms and Conditions (https://onlinelibrary.wiley.com/terms-and-conditions) on Wiley Online Library for rules of use; OA articles are governed by the applicable Creative Commons License

2199160x, 2022, 7, Downloaded from https://onlinelibrary.wiley.com/doi/10.1002/aelm.202101126 by Bibliotheek Rijksuniversiteit, Wiley Online Library on [18/01/2023]. See the Terms and Conditions (https://onlinelibrary.wiley.com/terms-and-conditions) on Wiley Online Library for rules of use; OA articles are governed by the applicable Creative Commons License

such as navigation, night vision, and telecommunication.[6] However, the near-infrared (NIR) region is not readily and cost-effectively covered by traditional inorganic semiconductors; and the organic semiconductor contenders in this spectral region remain rather elusive.[7]

NIR light-emitting devices are therefore an important avenue for applications of CQDs. Typically, electroluminescent devices use the light-emitting diode (LED) configuration, which have shown great improvement in the last years.[8] However, in the context of downscaling the pixels, a different device geometry emerges as an attractive alternative, namely light-emitting field-effect transistors (LEFETs), which offer the possibility to combine electroluminescence generation and electrical switching function within one device.[6]

The first NIR-emitting LEFET based on CQDs (CQD LEFET) was based on PbS.[9] This device employed a film of PbS CQDs capped with 3-mercaptopropionic acid (MPA) and was gated with an ion gel. The maximum external quantum efficiency (EQE) was reported to be 2×10^{-5}, which was comparable with the one of LEDs fabricated with the same material at the time of publication. The next notable step was an ambipolar CQD LEFET based on PbS CQDs capped with tetrabutylammonium iodide (TBAI), which used a solid gate dielectric.[10] Iodide ligands provide better passivation of the CQD surface than MPA, leading to an improvement of the electroluminescence EQE up to 1.3×10^{-5} at room temperature and of 1% below 100K. Importantly, these results were obtained using a device structure with a solid-state gate dielectric having a lower capacitance than the ion gel used in the above-mentioned pioneering work (vide infra).

However, two common issues are limiting the device performance in both above-mentioned PbS CQD LEFETs: i) the layer-by-layer approach used for the CQD film deposition and ii) the unbalanced ambipolar charge transport of the active layer.

The layer-by-layer deposition has been a widely employed method for the formation of conductive CQD films by replacing the long insulating native ligands with shorter ones using a solid-state reaction.[11] Besides being a time-intensive and wasteful process, this method leads to defects in the film and the formation of trap states at the CQD surface, which deteriorate both the light-emission properties and the charge transport in the active layer.[12] Recently, a new method has been developed to substitute the long insulating native ligands, the so-called phase-transfer ligand exchange (PTLE), which allows to make a stable colloidal dispersion (an ink) of QDs decorated by short ligands.[13,14] This ink can then be used for a single-step deposition of conductive CQD films by various techniques and thus is much more attractive for the development of CQD-based technologies.[15,16]

The second problem is much more fundamental. The majority of PbS CQDs synthetic methods result in nonstoichiometric, Pb-rich particles,[17–19] which give rise to n-type behavior of the films.[20] It has been demonstrated that tuning the size of the CQDs and changing the nature of the capping ligands the degree of the n-doping can be adjusted,[21] but obtaining PbS CQD films with highly balanced ambipolar transport from an ink is still an open challenge.

Here we demonstrated the first PbS CQD LEFET fabricated from colloidally ligand-exchanged inks, consisting of PbS CQDs capped with the widely used methylammonium lead iodide-like coating. We utilized a bilayer structure where on top of the n-type CQD film we deposited a network of polymer wrapped single-walled semiconducting carbon nanotubes (CNTs).[22,23] The heterostructure shows a well-balanced ambipolar transport and almost identical hole and electron linear mobilities ($0.2\ cm^2\ V^{-1}\ s^{-1}$). The EQE of the resulting device was found to be 1.2×10^{-4}, which is almost an order of magnitude higher compared to the previously reported PbS CQD LEFETs.

2. Results and Discussion

The CQD LEFETs were fabricated on borosilicate glass substrates where gold source/drain electrodes were lithographically defined and the gate dielectric ($PMMA/Al_2O_3$) and electrode were deposited on top of the active layer, defining a bottom contact/top gate FET configuration (see schematic in **Figure 1**A). The CQD active layer was deposited by spin-coating an ink of methylammonium lead iodide ($MAPbI_3$) coated PbS CQDs in 2,6-difluoropyridine (DFP). This is, to our knowledge, the first example of CQD LEFETs fabricated using a CQD ink, namely without using the layer-by-layer coating method. $MAPbI_3$ coating provides efficient electronic passivation of PbS CQDs and photoluminescence quantum yield of PbS-$MAPbI_3$ inks is 20–30%, comparable with the quantum yields of CQDs capped with oleic acid before the ligand exchange.[24–26] The TEM image of the PbS-$MAPbI_3$ CQDs is shown in Figure S1 (Supporting Information).

DFP is chosen as a solvent because it allows high colloidal stability of the PbS-$MAPbI_3$ CQDs ink.[27] As mentioned, the gate dielectric is deposited onto the CQD film and consists of 10 nm of poly(methyl methacrylate) (PMMA) deposited by spin coating and 80 nm of Al_2O_3, grown by atomic layer deposition (ALD). The PMMA interlayer is necessary to prevent chemical degradation of the CQDs upon exposure to the highly reactive trimethylaluminum during the ALD of Al_2O_3.[10] Also, the thin PMMA layer serves as an adhesion layer between the CNTs network and the oxide layer and ensures a low density of trap states at the semiconductor-dielectric interface.[28] Finally, the device is finished by evaporating the gate electrode through a shadow mask (see Figure S2, Supporting Information, for the optical images of devices). The fabrication of CQD-CNTs LEFETs differed only in the deposition by blade-coating of a CNTs network onto the CQD film. Excellent compatibility of CQDs and CNTs as a complementary pair of semiconducting materials was previously shown during the fabrication of high-performance ambipolar inverters.[29] The CNTs ink consists of poly(3-dodecylthiophene-2,5-diyl)-wrapped (P3DDT) semiconducting CNTs, prepared by using our previously published method.[30] P3DDT-wrapped semiconducting CNTs exhibit strong p-type electronic transport properties but depending in the preparation method they can still show a substantial electron mobility.[23,31] More details on CQD ink preparation and device fabrication can be found in the Experimental section.

The output characteristics of LEFETs fabricated using solely PbS-$MAPbI_3$ as active layer reveal ambipolar transport with the dominance of negative charge carriers (Figure 1B). The transfer curves (Figure 1C) show more clearly the strongly electron-dominated ambipolar transport, with a linear electron mobility of about $5.2 \times 10^{-3}\ cm^2\ V^{-1}\ s^{-1}$ which is in a good agreement with literature reports.[27,32] The meaningful values of hole

 © 2022 The Authors. Advanced Electronic Materials published by Wiley-VCH GmbH

2199160x, 2022, 7, Downloaded from https://onlinelibrary.wiley.com/doi/10.1002/aelm.202101126 by Bibliotheek Rijksuniversiteit, Wiley Online Library on [18/01/2023]. See the Terms and Conditions (https://onlinelibrary.wiley.com/terms-and-conditions) on Wiley Online Library for rules of use; OA articles are governed by the applicable Creative Commons License

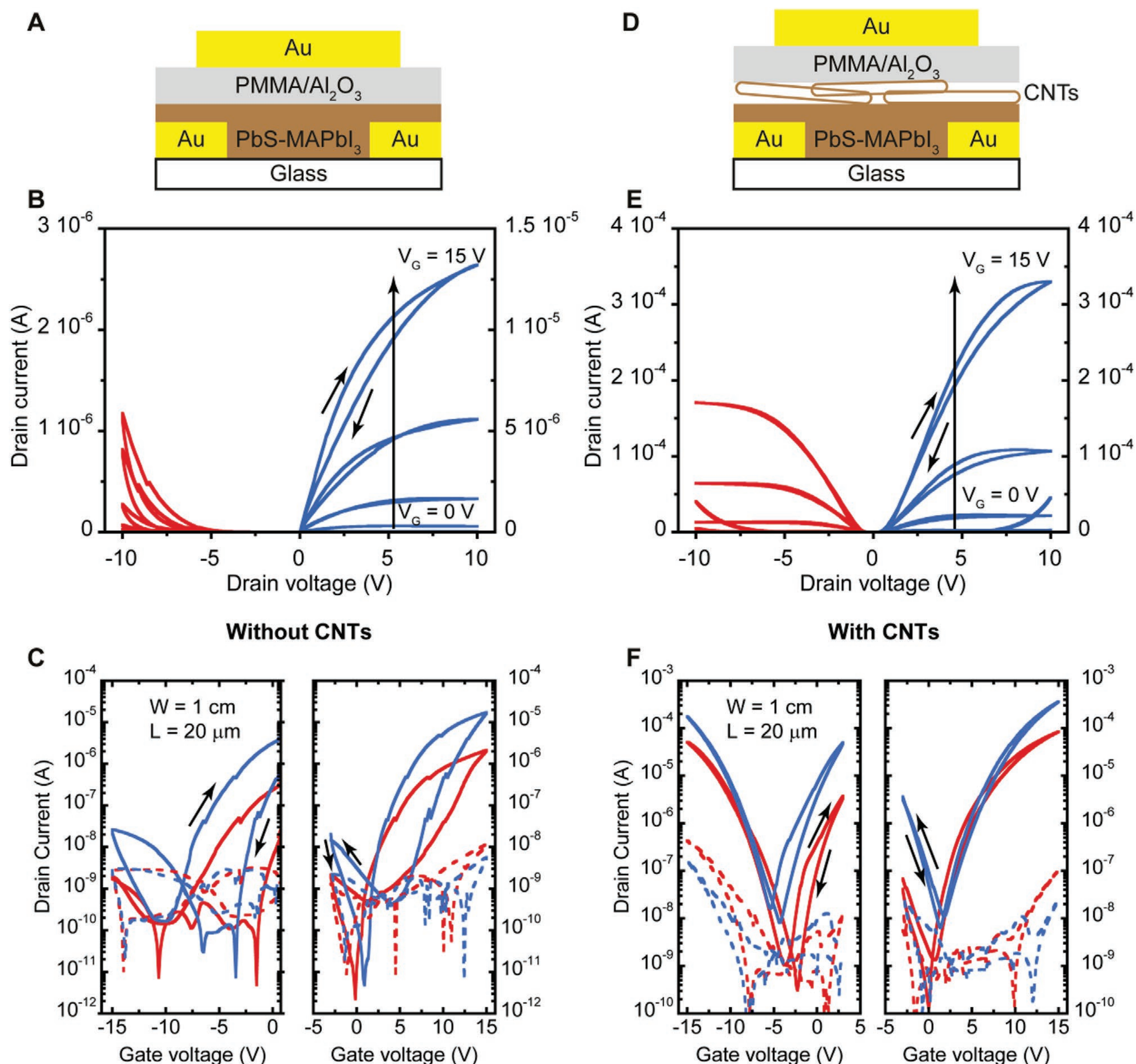

Figure 1. A) Schematic of CQD LEFET and B) resulting output characteristics. C) Transfer characteristics of CQD LEFETs, the sweeps are measured at drain voltage equal to 2 V (red) and 5 V (blue). Dashed lines represent the gate current D) schematic of CQD-CNTs LEFET and E) resulting output characteristics. F) Transfer characteristics of CQD-CNTs LEFETs, the sweeps are measured at drain voltage equal to 2 V (red) and 5 V (blue). Dashed lines represent the gate current.

mobility could not be extracted because the drain current and gate leakage current were comparable. The fabrication of LEFETs with an active layer with such imbalanced electron and hole transport will hamper the possibility to achieve high electroluminescence quantum efficiency. It has been demonstrated in the case of organic semiconductors, that more balanced mobilities and therefore better LEFETs could be achieved when blending hole and electron transport materials[33,34] or when a heterostructure of the two is fabricated.[35]

We therefore adopted a similar strategy by fabricating a heterostructure using the electron transporting PbS-$MAPbI_3$ and the hole transporting polymer-wrapped CNTs.

The schematic structure of the CQD-CNTs LEFETs is shown in Figure 1D. A network of polymer-wrapped semiconducting nanotubes is deposited on top of the CQD layer before the gate dielectric. This is possible due to the orthogonality of the solvents employed for the deposition of the two semiconductors (DFP and *o*-xylene for the CQDs and the CNTs, respectively).

When the gate voltage is applied, the conductive channel is created nearby the gate dielectric. As the CNT layer has a thickness of few nanometers, the channel is formed at the interface between the two materials, involving both of them in the transport (vide infra).[36] This results in almost ideally balanced ambipolar output characteristics (Figure 1E). The

 © 2022 The Authors. Advanced Electronic Materials published by Wiley-VCH GmbH

hole channel's saturation current becomes almost equal to the one of the electron channel for the same absolute value of the gate voltage. This is important because the working principle of LEFETs is based on the creation of an ambipolar regime, when one electrode injects holes and the other electrons into the channel.[6] Recombination of electrons and holes with subsequent light emission occurs at the meeting point of two subchannels (recombination zone). Even taking into account the unavoidable diffusion, the recombination zone of LEFETs is typically much narrower than the width of the transistor channel.[10] The position of the recombination zone in the channel can be moved by tuning the applied drain and gate voltages. This confirms the "truly ambipolar" nature of a device with coexisting electron and hole channels which is essential for light-emission efficiency.[37] Positioning the recombination zone further away from the electrodes helps to suppress electrode-induced exciton recombination as well as carrier extraction at the electrodes.[6,37,38]

Figure 1F shows the transfer characteristics of the CQD-CNT LEFETs representing a typical V-shape transfer curve for ambipolar transistors and confirming the well-balanced transport of the device. The inclusion of the CNTs resulted in more balanced characteristics, higher drain current and similar on/off current ratio for both charge carriers. Furthermore, the position of the off state in the CQD-CNT LEFETs is almost equal for forward and reverse scanning directions, which is not the case for CQD devices that are affected by large hysteresis. Noteworthy, the hysteresis in the CQD-CNT device is much less pronounced, especially for holes. Such a small hysteresis for holes is atypical for PbS CQD films, which usually display

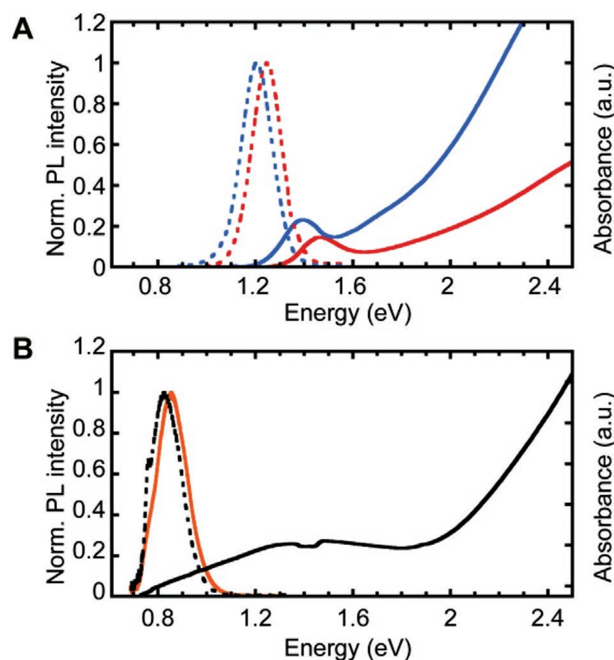

Figure 2. A) Absorption and photoluminescence spectra of oleate-capped PbS CQDs in hexane (red solid and dashed lines) and capped with $MAPbI_3$ in DFP (blue solid and dashed lines). B) Absorption and photoluminescence spectra of CQD-CNT heterostructure (black solid and dashed lines) as well as electroluminescence spectrum of CQD-CNT LEFETs (orange).

pronounced hole trapping. This is a further indication that the hole transport in our heterostructure is occurring through the CNT network. The extracted values of the linear mobility for holes and electrons are about 0.2 $cm^2 V^{-1} s^{-1}$, which shows 2 orders of magnitude enhancement of the electron mobility compared to those obtained for PbS CQD only LEFET. The increase of the electron mobility should also be assign to the beneficial role of the CNTs, transistors made with similar CNT inks display hole mobility of 1 $cm^2 V^{-1} s^{-1}$ and electron mobility of 0.4 $cm^2 V^{-1} s^{-1}$.[30]

When considering electroluminescent devices, the optical properties of the emitting material need special attention. The summary of the optical properties of the employed PbS CQDs is shown in **Figure 2**A. The starting dispersion of PbS CQDs capped with native oleic acid (OA) ligands in hexane has the first excitonic peak position at 1.47 eV. Upon ligand-exchange with $MAPbI_3$ and redispersion in DFP, this peak shifts to 1.4 eV, which is typically explained by the difference in dielectric permittivity of the solvents (1.9 for hexane and 107.8 for DFP) and lowering of the quantum confinement of the CQDs after the ligand exchange.[27,39] The same trend is observed with the emission spectra.

The emission spectrum of the CQD-CNT heterostructure shows a single peak originating from the CQD layer (Figure 2B), while the emission of the CNTs is not detectable (see Figure S3, Supporting Information; the emission spectrum of CNTs has a series of distinct sharp peaks due to the presence of CNTs with different diameter and thus different bandgap). This is due to the very small amount of CNTs present in the ≈3–6 nm layer and their limited quantum yield, which is much lower than the one of the CQD layer.[40,41]

The CQD-CNT film exhibits the maximum photoluminescence at 0.83 eV (Figure 2B). The origin of such a pronounced red-shift of the emission in films compared to the one from the ink is attributed to the further loss of quantum confinement of CQDs at the elevated temperature of the deposition process.[42,43] The absorption spectrum of the CQD-CNT film is shown in Figure 2B. The spectrum shows a large broadening in the low energy region, most probably attributable to the weakening of the quantum confinement.[10,42]

The CQD film is subjected to elevated temperature during the blade-coating deposition of the CNTs (70 °C), the ALD dielectric growth ($T = 100$ °C) and the post-annealing of the device, which is performed at 140 °C. The feature at 0.75 eV in the emission spectrum is an artifact originated by the drop of the sensitivity of the detectors for low energy photons. It is useful to note that PbS-$MAPbI_3$ ink in DFP and the corresponding CQD film show almost identical full width at half-maximum of the emission peaks (0.22 eV).

The EL maximum for the CQD-CNT LEFET is at 0.86 eV (Figure 2B). The small discrepancy between the peak positions of the electro- and photoluminescence can likely be explained by the state filling of the transport levels at higher carried densities.[10] We note that in line with their inferior electrical properties, LEFETs solely comprising CQDs in the active layer only offer faint EL.

The dependence of the drain current versus the gate voltage is shown in **Figure 3**A. The light-emission measurements were performed inside a dark chamber, where the LEFET was placed right onto the calibrated photodiode and was electrically

 © 2022 The Authors. Advanced Electronic Materials published by Wiley-VCH GmbH

2199160x, 2022, 7, Downloaded from https://onlinelibrary.wiley.com/doi/10.1002/aelm.202101126 by Bibliotheek Rijksuniversiteit, Wiley Online Library on [18/01/2023]. See the Terms and Conditions (https://onlinelibrary.wiley.com/terms-and-conditions) on Wiley Online Library for rules of use; OA articles are governed by the applicable Creative Commons License

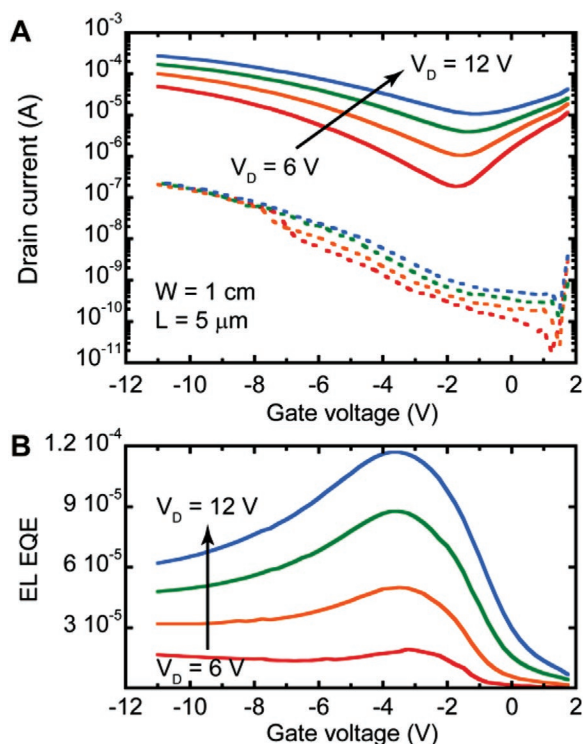

Figure 3. A) Drain current of the CQD-CNT LEFET versus the gate voltage (solid lines) and gate leakage current (dashed lines). B) EQE of electroluminescence of the same device as a function of the applied electrode potentials.

connected via probes to the semiconducting analyzer.[9] This measurement configuration obviously underestimates the EQE due to impossibility to collect all the emitted light in the used geometry. The maximum light emission in the device was measured by applying a positive drain voltage and negative gate bias (Figure 3B). The absolute value of the EQE increases with the applied drain voltage, fact previously attributed to the filing of the trap states in the channel.[10] The maximum value measured for the EQE is 1.2×10^{-4} which is almost an order of magnitude higher compared to the previous record in NIR-emitting CQD-based LEFETs at room temperature (see **Table 1**).

This improvement of the EL EQE is determined by the combination of two factors. First, the balanced ambipolar charge transport achieved combining the n-type CQD layer with the p-type dominated polymer-wrapped semiconducting CNTs layer. Second, the utilization of liquid phase-transfer ligand exchange instead of the layer-by-layer solid-state reaction, which exhibit improved surface passivation of CQDs.

3. Conclusions

By combining an n-type layer of PbS CQDs with a p-type layer of polymer-wrapped semiconducting CNTs we obtained a well-balanced ambipolar transport, which show to be key to improve the external quantum efficiency of the light-emitting device. Linear hole and electron mobilities up to 0.2 $cm^2 V^{-1} s^{-1}$ are measured in the heterostructure using $PMMA/Al_2O_3$ as gate dielectric. These devices exhibited electroluminescence emission maximum at 0.86 eV (1440 nm), with maximum external quantum efficiency of the electroluminescence is 1.2×10^{-4}, that is almost an order of magnitude higher compared to previous reports on PbS CQD LEFETs. Interestingly, while the CNTs appear very important for the electrical performance of the device, we did not find measurable signature of their EL.

Future work should focus on optimization of CQD LEFET structure to favor light extraction and to apply strategies to reduce trapping states.

4. Experimental Section

PbS CQDs Synthesis: All the solvents and reagents were analytically pure and were used without further purification. Synthesis and isolation of PbS CQDs capped with oleic acid was performed by using a hot-injection method as described except for the amount of OA (56 mL instead of 70 mL) and injection at a lower temperature (80 °C).[44]

Preparation of the Inks: Solution-phase ligand exchange was performed by using a previously published method.[27] $MAPbI_3$ solution in *N*-methylformamide was prepared by mixing PbI_2 and MAI in 1:1 molar ratio. In a typical procedure, 10 mL of *N*-methylformamide solution of 50×10^{-3} M $MAPbI_3$ was combined with 10 mL of oleate-capped PbS CQDs in hexanes with a concentration of 5 mg mL^{-1}. The mixture was stirred by using a magnetic stirring bar until all the CQDs are transferred into a polar phase. Then the top phase was discarded and the bottom phase was washed thrice with hexanes. Ligand-exchanged CQDs were precipitated by addition of acetone, collected by centrifugation and finally re-dispersed in DFP to form an ink. For electron microcopy analyses, the diluted ink was dropcasted on a carbon-coated copper grid. The images were recorded with a double aberration corrected FEI Themis Z microscope operated at 300 kV using the previously reported parameters.[42]

Device Fabrication: 0.7 mm thick borosilicate glass substrates were cleaned with detergent and then consequently ultrasonicated in deionized water, acetone and isopropanol and dried in oven at 120 °C for at least 20 min. Then the source and drain electrodes consisting from 3 nm of Ti and 37 nm of Au were patterned by using UV lithography. The substrates were treated with O_2-plasma for 3 min before the CQD film deposition. CQD film was deposited by spin-coating PbS-$MAPbI_3$ ink in DFP inside the N_2-filled glove box at 1000 rpm resulting in about 50 nm film. A network of semiconducting CNTs was deposited by blade-coating two layers of CNT ink at 70 °C with 3 mm s^{-1} blade speed. The CNT ink consisted of poly(3-dodecylthiophene-2,5-diyl)-wrapped (P3DDT) semiconducting CNTs and was prepared using the method as described

Table 1. Overview of the performance and device structure of the NIR-emitting CQD-based LEFETs.

Active layer	EL max [nm]	EQE	Dielectric	Mobility [$cm^2 V^{-1} s^{-1}$]	Reference
PbS-MPA	≈1480	2×10^{-5}	[EMIM][FAP]	$\mu_h = 0.003–0.009$ $\mu_e = 0.04–0.06$	[9]
PbS-TBAI	1480	1.3×10^{-5}	$PMMA/Al_2O_3$	μ_h undetermined $\mu_e = 0.06$	[10]
PbS-$MAPbI_3$/CNTs	1490	1.2×10^{-4}	$PMMA/Al_2O_3$	$\mu_h = 0.2$ $\mu_e = 0.2$	This work

© 2022 The Authors. Advanced Electronic Materials published by Wiley-VCH GmbH

2199160x, 2022, 7, Downloaded from https://onlinelibrary.wiley.com/doi/10.1002/aelm.202101126 by Bibliotheek Rijksuniversiteit, Wiley Online Library on [18/01/2023]. See the Terms and Conditions (https://onlinelibrary.wiley.com/terms-and-conditions) on Wiley Online Library for rules of use; OA articles are governed by the applicable Creative Commons License

in a previously published work.[30] Such deposition conditions results in in the ≈3–6 nm layer on a flat SiO_2 surface. Then an ≈10 nm PMMA layer was spin-coated from 6 mg mL^{-1} solution in acetonitrile at 3000 rpm and dried on a hotplate for 1 min at 120 °C. The gate dielectric was finished by growing 80 nm of aluminum oxide at 100 °C by atomic layer deposition from trimethylaluminum and water precursors (Picosun R200 advanced deposition system). Finally, the device fabrication was finished by thermal evaporation of gold gate electrode through a shadow mask. The device was annealed for 20 min at 140 °C inside the N_2-filled glove box.

LEFET Characterization: The capacitance of the gate dielectric on indium tin oxide (ITO)/PMMA/Al_2O_3/Al devices was measured using Solarton 1260 impedance gain-phase analyzer. Electrical characterization of the CQD LEFET was done using a Keithley 4200-SCS semiconductor parameter analyzer. Absorption spectra were recorded using a Shimadzu UV-3600 spectrometer. Electroluminescence and photoluminescence spectra were collected using a spectrometer and recorded by an Andor iDus 1.7 µm InGaAs camera. PL spectra were measured by exciting the sample with the second harmonic (400 nm) of a mode-locked Ti:sapphire laser (Mira 900, Coherent). For the EQE measurements, the response of calibrated photodiode to the emitted light from the LEFETs was measured. The EQE was calculated by using the following formula

$$EQE = \frac{I_{\text{diode}}}{I_{\text{d}}} \cdot \frac{1}{S_{\text{av}}} \cdot \frac{e}{hc} \cdot \frac{\int \lambda \cdot EL_{\text{norm}}(\lambda) d\lambda}{\int EL_{\text{norm}}(\lambda) d\lambda} \quad (1)$$

where I_{diode} is the recorded current by a calibrated photodiode and S_{av} is the average sensitivity of this photodiode, I_d is the source-drain current of a transistor.

Supporting Information

Supporting Information is available from the Wiley Online Library or from the author.

Acknowledgements

The authors are thankful to A. Kamp and T. Zaharia for the technical support. The Groningen team is grateful for the financial support of the Dieptestrategie program from Zernike Institute for Advanced Materials. This work was financed through the Materials for Sustainability (Mat4Sus) program (739.017.005) of the Netherlands Organisation for Scientific Research (NWO). S.K. acknowledges the Deutsche Forschungsgemeinschaft (DFG) for a postdoctoral research fellowship (408012143).

Conflict of Interest

The authors declare no conflict of interest.

Data Availability Statement

Research data are not shared.

Keywords

carbon nanotubes, colloidal quantum dots, electroluminescence, field-effect transistors, lead sulfide, light emission

Received: October 15, 2021
Revised: January 25, 2022
Published online: February 25, 2022

[1] C. B. Murray, C. R. Kagan, M. G. Bawendi, *Annu. Rev. Mater. Sci.* **2000**, *30*, 545.
[2] D. V. Talapin, J.-S. Lee, M. V. Kovalenko, E. V. Shevchenko, *Chem. Rev.* **2010**, *110*, 389.
[3] C. R. Kagan, E. Lifshitz, E. H. Sargent, D. V. Talapin, *Science* **2016**, *353*, aac5523.
[4] M. A. Hines, G. D. Scholes, *Adv. Mater.* **2003**, *15*, 1844.
[5] I. Moreels, Y. Justo, B. De Geyter, K. Haustraete, J. C. Martins, Z. Hens, *ACS Nano* **2011**, *5*, 2004.
[6] S. Kahmann, A. Shulga, M. A. Loi, *Adv. Funct. Mater.* **2019**, *30*, 1904174.
[7] H. Lu, G. M. Carroll, N. R. Neale, M. C. Beard, *ACS Nano* **2019**, *13*, 939.
[8] S. Pradhan, F. Di Stasio, Y. Bi, S. Gupta, S. Christodoulou, A. Stavrinadis, G. Konstantatos, *Nat. Nanotechnol.* **2019**, *14*, 72.
[9] J. Schornbaum, Y. Zakharko, M. Held, S. Thiemann, F. Gannott, J. Zaumseil, *Nano Lett.* **2015**, *15*, 1822.
[10] A. G. Shulga, S. Kahmann, D. N. Dirin, A. Graf, J. Zaumseil, M. V. Kovalenko, M. A. Loi, *ACS Nano* **2018**, *12*, 12805.
[11] H. Beygi, S. A. Sajjadi, A. Babakhani, J. F. Young, F. C. J. M. van Veggel, *Appl. Surf. Sci.* **2018**, *459*, 562.
[12] D. M. Balazs, M. A. Loi, *Adv. Mater.* **2018**, *30*, 1800082.
[13] M. V. Kovalenko, M. Scheele, D. V. Talapin, *Science* **2009**, *324*, 1417.
[14] A. Fischer, L. Rollny, J. Pan, G. H. Carey, S. M. Thon, S. Hoogland, O. Voznyy, D. Zhitomirsky, J. Y. Kim, O. M. Bakr, E. H. Sargent, *Adv. Mater.* **2013**, *25*, 5742.
[15] J. Jean, J. Xiao, R. Nick, N. Moody, M. Nasilowski, M. Bawendi, V. Bulović, *Energy Environ. Sci.* **2018**, *11*, 2295.
[16] Q. Lin, H. J. Yun, W. Liu, H.-J. Song, N. S. Makarov, O. Isaienko, T. Nakotte, G. Chen, H. Luo, V. I. Klimov, J. M. Pietryga, *J. Am. Chem. Soc.* **2017**, *139*, 6644.
[17] M. A. M. A. Hines, G. D. G. D. Scholes, *Adv. Mater.* **2003**, *15*, 1844.
[18] M. P. Hendricks, M. P. Campos, G. T. Cleveland, I. Jen-La Plante, J. S. Owen, *Science* **2015**, *348*, 1226.
[19] L. Cademartiri, E. Montanari, G. Calestani, A. Migliori, A. Guagliardi, G. A. Ozin, *J. Am. Chem. Soc.* **2006**, *128*, 10337.
[20] D. Kim, D.-H. Kim, J.-H. Lee, J. C. Grossman, *Phys. Rev. Lett.* **2013**, *110*, 196802.
[21] P. R. Brown, D. Kim, R. R. Lunt, N. Zhao, M. G. Bawendi, J. C. Grossman, V. Bulović, *ACS Nano* **2014**, *8*, 5863.
[22] J. M. Salazar-Rios, W. Talsma, V. Derenskyi, W. Gomulya, T. Keller, M. Fritsch, S. Kowalski, E. Preis, M. Wang, S. Allard, G. C. Bazan, U. Scherf, M. C. dos Santos, M. A. Loi, *Small Methods* **2018**, *2*, 1700335.
[23] V. Derenskyi, W. Gomulya, J. M. S. Rios, M. Fritsch, N. Fröhlich, S. Jung, S. Allard, S. Z. Bisri, P. Gordiichuk, A. Herrmann, U. Scherf, M. A. Loi, *Adv. Mater.* **2014**, *26*, 5969.
[24] D. N. Dirin, S. Dreyfuss, M. I. Bodnarchuk, G. Nedelcu, P. Papagiorgis, G. Itskos, M. V. Kovalenko, *J. Am. Chem. Soc.* **2014**, *136*, 6550.
[25] Z. Yang, J. Z. Fan, A. H. Proppe, F. P. G. De Arquer, D. Rossouw, O. Voznyy, X. Lan, M. Liu, G. Walters, R. Quintero-Bermudez, B. Sun, S. Hoogland, G. A. Botton, S. O. Kelley, E. H. Sargent, *Nat. Commun.* **2017**, *8*, 1325.
[26] W. Wang, M. Zhang, Z. Pan, G. M. Biesold, S. Liang, H. Rao, Z. Lin, X. Zhong, *Chem. Rev.* **2021**, acs. chemrev.1c00478.
[27] D. Bederak, N. Sukharevska, S. Kahmann, M. Abdu-Aguye, H. Duim, D. N. Dirin, M. V. Kovalenko, G. Portale, M. A. Loi, *ACS Appl. Mater. Interfaces* **2020**, *12*, 52959.
[28] M. Held, S. P. Schießl, D. Miehler, F. Gannott, J. Zaumseil, *Appl. Phys. Lett.* **2015**, *107*, 083301.
[29] A. G. Shulga, V. Derenskyi, J. M. Salazar-Rios, D. N. Dirin, M. Fritsch, M. V. Kovalenko, U. Scherf, M. A. Loi, *Adv. Mater.* **2017**, *29*, 1701764.

© 2022 The Authors. Advanced Electronic Materials published by Wiley-VCH GmbH

2199160x, 2022, 7, Downloaded from https://onlinelibrary.wiley.com/doi/10.1002/aelm.202101126 by Bibliotheek Rijksuniversiteit, Wiley Online Library on [18/01/2023]. See the Terms and Conditions (https://onlinelibrary.wiley.com/terms-and-conditions) on Wiley Online Library for rules of use; OA articles are governed by the applicable Creative Commons License

[30] W. Talsma, A. A. Sengrian, J. M. Salazar-Rios, H. Duim, M. Abdu-Aguye, S. Jung, S. Allard, U. Scherf, M. A. Loi, *Adv. Electron. Mater.* **2019**, *5*, 1900288.
[31] S. Z. Bisri, J. Gao, V. Derenskyi, W. Gomulya, I. Iezhokin, P. Gordiichuk, A. Herrmann, M. A. Loi, *Adv. Mater.* **2012**, *24*, 6147.
[32] D. M. Balazs, N. Rizkia, H.-H. H. Fang, D. N. Dirin, J. Momand, B. J. Kooi, M. V. Kovalenko, M. A. Loi, *ACS Appl. Mater. Interfaces* **2018**, *10*, 5626.
[33] M. A. Loi, C. Rost-Bietsch, M. Murgia, S. Karg, W. Riess, M. Muccini, *Adv. Funct. Mater.* **2006**, *16*, 41.
[34] C. Rost, S. Karg, W. Riess, M. A. Loi, M. Murgia, M. Muccini, *Appl. Phys. Lett.* **2004**, *85*, 1613.
[35] F. Dinelli, R. Capelli, M. A. Loi, M. Murgia, M. Muccini, A. Facchetti, T. J. Marks, *Adv. Mater.* **2006**, *18*, 1416.
[36] A. G. Shulga, L. Piveteau, S. Z. Bisri, M. V. Kovalenko, M. A. Loi, *Adv. Electron. Mater.* **2016**, *2*, 1500467.
[37] J. Zaumseil, R. H. Friend, H. Sirringhaus, *Nat. Mater.* **2006**, *5*, 69.
[38] C. Santato, R. Capelli, M. A. Loi, M. Murgia, F. Cicoira, V. A. L. Roy, P. Stallinga, R. Zamboni, C. Rost, S. F. Karg, M. Muccini, *Synth. Met.* **2004**, *146*, 329.
[39] T. Takagahara, *Phys. Rev. B* **1993**, *47*, 4569.
[40] W. Gomulya, G. D. Costanzo, E. J. F. de Carvalho, S. Z. Bisri, V. Derenskyi, M. Fritsch, N. Fröhlich, S. Allard, P. Gordiichuk, A. Herrmann, S. J. Marrink, M. C. dos Santos, U. Scherf, M. A. Loi, *Adv. Mater.* **2013**, *25*, 2948.
[41] X. Wei, T. Tanaka, S. Li, M. Tsuzuki, G. Wang, Z. Yao, L. Li, Y. Yomogida, A. Hirano, H. Liu, H. Kataura, *Nano Lett.* **2020**, *20*, 410.
[42] N. Sukharevska, D. Bederak, V. M. Goossens, J. Momand, H. Duim, D. N. Dirin, M. V. Kovalenko, B. J. Kooi, M. A. Loi, *ACS Appl. Mater. Interfaces* **2021**, *13*, 5195.
[43] S. Kahmann, M. A. Loi, *Appl. Phys. Rev.* **2020**, *7*, 041305.
[44] M. Yarema, O. Yarema, W. M. M. Lin, S. Volk, N. Yazdani, D. Bozyigit, V. Wood, *Chem. Mater.* **2017**, *29*, 796.

© 2022 The Authors. Advanced Electronic Materials published by Wiley-VCH GmbH

2199160x, 2022, 7, Downloaded from https://onlinelibrary.wiley.com/doi/10.1002/aelm.202101126 by Bibliotheek Rijksuniversiteit, Wiley Online Library on [18/01/2023]. See the Terms and Conditions (https://onlinelibrary.wiley.com/terms-and-conditions) on Wiley Online Library for rules of use; OA articles are governed by the applicable Creative Commons License